Moreover, GMRES-RP is the most efficient, and CGS-RP is the least efficient.

REFERENCES

[1] L. Tsang, J. A. Kong, K.-H. Ding, and C. O. Ao, *Scattering of Electromagnetic Waves – Numerical Simulations*. New York, NY, USA: Wiley, 2001.

[2] G. D. Yang and Y. Du, "A robust preconditioned GMRES method for electromagnetic scattering from dielectric rough surfaces," *IEEE Trans. Geosci. Remote Sens.*, vol. 50, no. 9, pp. 3396–3408, 2012.

[3] J. T. Johnson, R. J. Burkholder, J. V. Toporkov, D. R. Lyzenga, and W. J. Plant, "A numerical study of the retrieval of sea surface height profiles from low grazing angle radar data," *IEEE Trans. Geosci. Remote Sens.*, vol. 47, no. 6, pp. 1641–1650, 2009.

[4] H. Ye and Y.-Q. Jin, "A hybrid analytic-numerical algorithm of scattering from an object above a rough surface," *IEEE Trans. Geosci. Remote Sens.*, vol. 45, no. 5, pp. 1174–1180, 2007.

[5] M. Zribi, A. L. Morvan-Quemener, M. Dechambre, and N. Baghdadi, "Numerical backscattering analysis for rough surfaces including a cloddy structure," *IEEE Trans. Geosci. Remote Sens.*, vol. 48, no. 5, pp. 2367–2374, 2010.

[6] D. Holliday, L. L. DeRaad, and G. J. St-Cyr, "Forward-backward: A new method for computing low-grazing angle scattering," *IEEE Trans. Antennas Propag.*, vol. 44, no. 5, pp. 722–729, 1996.

[7] A. Iodice, "Forward-backward method for scattering from dielectric rough surfaces," *IEEE Trans. Antennas Propag.*, vol. 50, no. 7, pp. 901–911, 2002.

[8] J. West and J. M. Sturm, "On iterative approaches for electromagnetic rough-surface scattering problems," *IEEE Trans. Antennas Propag.*, vol. 47, no. 8, pp. 1281–1288, 1999.

[9] D. Torrungrueng, J. T. Johnson, and H.-T. Chou, "Some issues related to the novel spectral acceleration (NSA) method for the fast computation of radiation/scattering from one-dimensional extremely large-scale quasiplanar structures," *Radio Sci.*, vol. 37, no. 2, Mar. 2002.

[10] K. Inan and V. B. Erturk, "Application of iterative techniques for electromagnetic scattering from dielectric random and reentrant rough surfaces," *IEEE Trans. Geosci. Remote Sens.*, vol. 44, no. 11, pp. 3320–3329, 2006.

[11] R. Barrett, M. Berry, T. F. Chan, J. Demmel, J. Donato, J. Dongarra, V. Eijkhout, R. Pozo, C. Romine, and H. Van der Vorst, *Templates for the Solution of Linear Systems: Building Blocks for Iterative Methods*, 2nd ed. Philadelphia, PA, USA: SIAM, 1994.

A Circularly Polarized Pattern Diversity Antenna for Hemispherical Coverage

Changjiang Deng, Yue Li, Zhijun Zhang, and Zhenghe Feng

Abstract—In this communication, a circularly polarized (CP) antenna is proposed for satellite communication applications. The proposed antenna consists of two parts. One part is in-phase-fed folded monopoles with omnidirectional CP radiation pattern, and the other part is sequential-fed L-shaped monopoles with broadside CP radiation pattern. By combining the two parts as a pattern diversity antenna, upper hemispherical coverage with left-handed circular polarization (LHCP) is achieved in a small volume of $0.38\lambda \times 0.38\lambda \times 0.071\lambda$ (λ is the free-space wavelength). A prototype of the proposed antenna operating at 1.575 GHz has been built and tested. The measured overlapping bandwidth for both the two patterns with -10-dB impedance bandwidth and 3-dB axial-ratio (AR) is 6.7% (1.515–1.62 GHz), also with high port isolation. In addition, the AR and gain coverage over the upper hemisphere is discussed in detail.

Index Terms—Circular polarization, hemispherical coverage, pattern diversity antenna, satellite communications.

I. INTRODUCTION

With the rapid progress in wireless technology, numerous antennas have been proposed for satellite communication and navigation applications. In these satellite systems, polarization and spatial coverage are of significant importance for effective data communication [1]. Circularly polarized (CP) antenna is widely used in satellite communication because it can provide a stable link between the transmitting and receiving antennas regardless of polarization misalignment [2]. Hemispherical coverage is preferred because tracking satellite is not needed [3]. Quadrifilar helix antenna (QHA) is a typical solution that meets CP wave and wide spatial coverage requirements and many QHA designs have been proposed [4]–[7]. However, low elevation angle coverage is satisfied at the cost of high profile and the bandwidth of QHA is typical narrow.

Pattern diversity antenna is known for mitigating multi-path fading. Owing to its low profile, complementary patterns and flexible configuration, pattern diversity antenna with broadside and omnidirectional patterns also opens up some interesting possibilities in satellite communication applications. The combination of both patterns may provide full dynamic spatial coverage over the entire upper hemisphere. Various types of pattern diversity antennas have been designed with
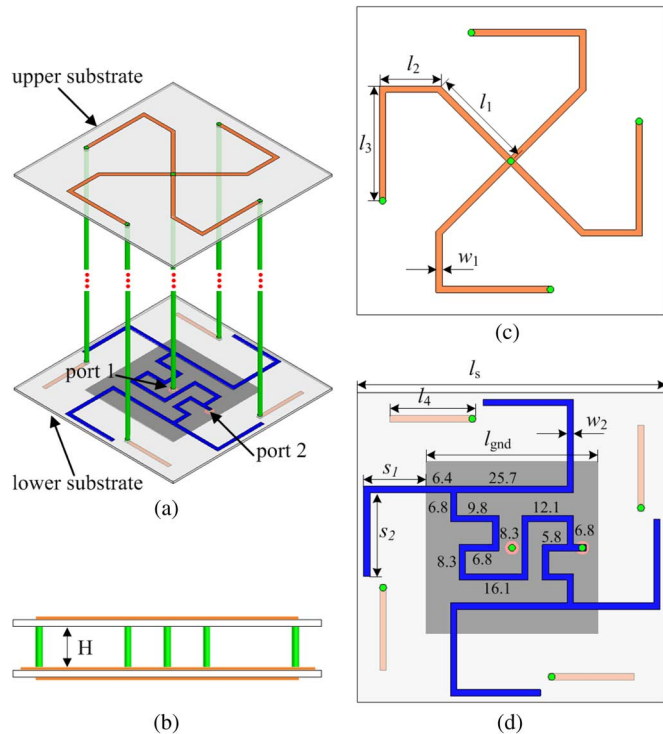
Fig. 1. Geometry and dimensions of the proposed diversity antenna (a) 3D view; (b) side view; (c) upper substrate; (d) lower substrate.

TABLE I
DETAILED DIMENSIONS (UNIT: mm)

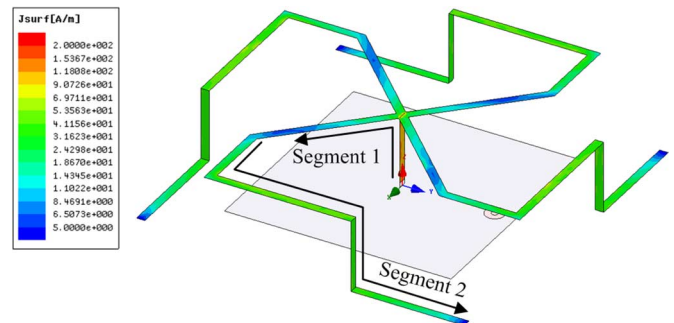| l_{gnd}	l_s	l_1	l_2	l_3	l_4
40	72	24	14.3	27	20
w_1	w_2	s_1	s_2	H	h
1.5	1.5	14.5	21	12	0.8

Fig. 2. Complex magnitude distribution of surface current on the four folded metallic strips at 1.575 GHz.

broadside and omnidirectional modes [8]–[13]. However, the polarization of antennas mentioned above is only linear polarization or the combination of linear polarization and circular polarization. In [14], a full CP diversity DRA is investigated for the first time. The CP pattern diversity DRA provides omnidirectional and broadside radiation patterns at 2.4 GHz. However, the profile is relatively high (about 0.17 λ), the weight is bulky, and the gain and axial ratio (AR) over the entire upper hemisphere are not well discussed.

The purpose of this communication is to propose a wideband and low-profile alternative of QHA for satellite communication applications. Hemispherical coverage is achieved by switching between the omnidirectional and broadside patterns of the proposed diversity antenna. Omnidirectional CP coverage is obtained by arranging four folded metallic strips rotationally symmetric along z-axis, which are fed by the same signal. Broadside CP coverage is obtained by feeding four rotationally symmetric, L-shaped monopoles with equal amplitude and incremental 90° phase delay. Compared with the design in [14], the size and weight of the proposed antenna design are reduced. Besides, dynamic spatial coverage is achieved over the entire upper hemisphere with AR < 3 dB.

II. ANTENNA DESIGN

A. Antenna Geometry

Fig. 1 shows the geometry of the proposed diversity antenna. The antenna consists of three parts: the upper FR4 ($\varepsilon_r = 4.4$, $\tan \delta = 0.02$) substrate, the lower FR4 substrate, and the air gap between them. Both of the two substrates have the same thickness ($h = 0.8$ mm) and the same size of $l_s \times l_s$. The thickness of the air gap is H. On the top layer of the upper substrate, four folded metallic strips are arranged in rotational symmetry and joined together at the centre. On the bottom layer of the lower substrate, four rotationally symmetrical metallic strips are connected to the corresponding metallic strips on the top layer of the

upper substrate via four metallic cylinders. Another metallic cylinder is placed at the centre along z-axis, which is used to feed the folded metallic strips. On the top layer of the lower substrate, a compact sequential-fed network, which was originally proposed in [15], is designed to provide four signals with equal amplitude and incremental 90° phase delay. Four rotationally symmetric L-shaped monopoles are connected to the corresponding feeding ports. The ground plane is on the bottom layer of the lower substrate, and the size is $l_{gnd} \times l_{gnd}$. The dimensions of the proposed diversity antenna are optimized by High Frequency Structure Simulator (HFSS) and the detailed values of each parameters are listed in Table I.

B. Operating Mechanism

The principle of omnidirectional circular polarization is analyzed first. Fig. 2 shows the complex magnitude distribution of surface current on four arms of the folded metallic strips. The cylinders are replaced by metallic strips for simplicity. It is shown that each of the four arms can be divided into segment 1 and segment 2 by the current null. The lengths of the two segments are about quarter-wavelength and half-wavelength, respectively. As segment 1 is near and above the ground plane, poor power will be radiated. The main radiators are the four segments 2. In [16], a pair of 45° tilted and orthogonally crossed dipole antennas is presented. CP wave can be generated in both directions on the array axis if the element space is quarter-wavelength. A further design is analyzed in [17], where a broadband omnidirectional CP pattern is achieved by loading four parasitic conducting strips on the sidewalls. In our design, the four segments 2 can be viewed as four tilt and crossed elements. As the four elements are rotationally placed and central-fed, the amplitudes and phases of the current on the four elements are identical. The space phase difference between elements can be obtained when observed in the horizontal orientation. Thus, by properly tuning the vertical and horizontal lengths of the four folded elements (which determine the amplitudes of the vertical and horizontal electric fields), and the elements spacing (which determines the space phase difference), Left-handed circular polarization (LHCP) can be generated in the horizontal plane.

Broadside circular polarization can be realized in various methods, such as using patch and ring. In this communication, the structure in [18] is adopted. The central sequential-fed network has a compact size
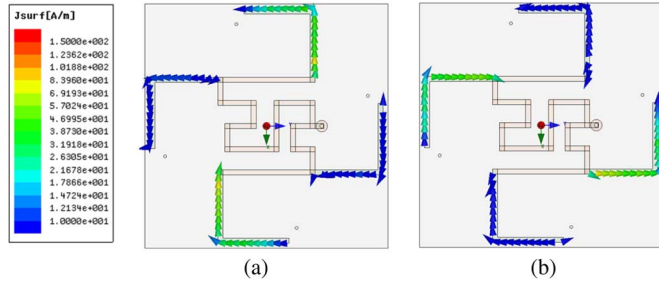
Fig. 3. Current distribution on four L-shaped monopoles at 1.575 GHz with different phases (a) $0°$; (b) $90°$.
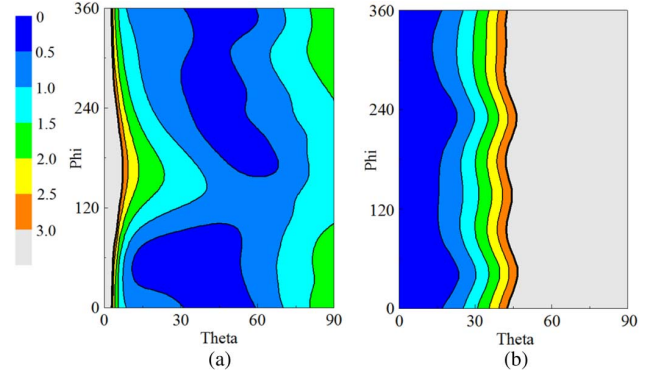

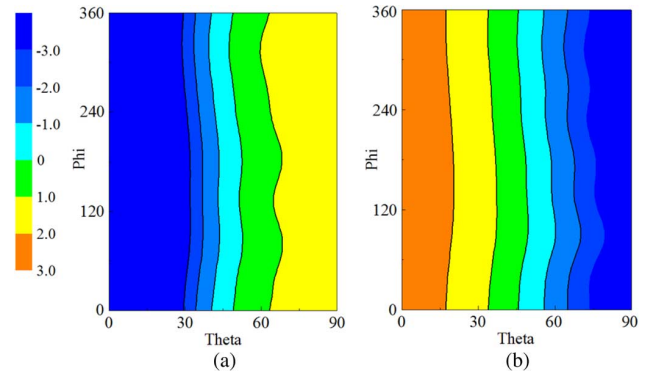Fig. 4. Simulated AR distribution at 1.575 GHz. (a) Omnidirectional pattern; (b) broadside pattern.

Fig. 5. Simulated LHCP gain distribution at 1.575 GHz. (a) Omnidirectional pattern; (b) broadside pattern.

of about $0.21\lambda \times 0.21\lambda$ and can provide four signals with equal amplitude and phases of $0°$, $90°$, $180°$, and $270°$ in a wide bandwidth. Fig. 3 shows the surface current distribution on four L-shaped monopoles with different phases. At moment $t = 0$, current is mainly concentrated on the surface of the two vertical monopoles with equal amplitude and phase difference of $180°$. Fig. 3(b) shows the moment $t = T/4$. A similar current distribution with equal amplitude and phase difference of $180°$ can be found on the surface of the two horizontal monopoles. Thus, broadside LHCP is generated.

C. Circularly Polarized Hemispherical Coverage

The ARs of omnidirectional and broadside modes for the upper hemisphere at 1.575 GHz are plotted in Fig. 4. It can be observed in Fig. 4(a) that the AR is less than 3 dB in the angle range of $\theta = 10° \sim 90°$ for omnidirectional pattern. Fig. 4(b) shows that the 3-dB AR criterion is satisfied from $\theta = 0°$ to $\theta = 40°$ for broadside pattern. If $\theta = 40°$ is used as the criterion of switching between omnidirectional pattern and broadside pattern, LHCP can be achieved over the entire hemisphere with AR < 3 dB. Fig. 5 shows the simulated LHCP gain distribution of both modes for the upper hemisphere at 1.575 GHz. It is shown in Fig. 5(a) that the LHCP gain is higher than -1 dBic in $\theta = 40° \sim 90°$ for omnidirectional pattern. Fig. 5(b) shows that the LHCP gain is higher than 0 dBic in $\theta = 0° \sim 40°$ for broadside pattern. Based on the criterion of $\theta = 40°$, the LHCP gain is higher than -1 dBic over the entire upper hemisphere, also with gain variation less than 4 dB.

D. Steps to Integrate the Proposed Antenna

The process of designing is summarized in this part to tune the diversity antenna and rescale to different frequency. As the proposed structure is an integration of two antennas, the steps of integration are listed separately.

Firstly, the design process of the omnidirectional pattern antenna element is given:
- Arrange four 0.75-wavelength strips in rotational symmetry and join them together at the centre for central excitation;
- Set the length proportion of segment 1 and 2 about 1:2;
- Tune the vertical and horizontal parts of the folded strips to optimize the amplitudes of the vertical and horizontal electric fields;
- Tune l_2 and the size of the ground plane to optimize the space phase difference between the four elements.

Then, the design process of the broadside pattern antenna element is given:
- Design a sequential-fed network to provide four ports with equal amplitude and incremental $90°$ phase delay;
- Connect four 0.25-wavelength L-shaped monopoles to the corresponding ports of the feeding network;

- Tune the length proportion of the L-shaped monopoles' two arms to get good AR at the broadside direction.

III. EXPERIMENTAL RESULTS

A prototype of the proposed antenna is fabricated and measured. Fig. 6 shows the assembled antenna. Five metallic cylinders are not only used to fix the two layers of substrates but also serve as conducting strips. In practical application, the cylinders can be replaced by metallic screws to support the two substrates firmly. Fig. 7 shows the measured S parameters, which agree well with the simulated results. The measured -10-dB impedance bandwidth of port 1 is 7.6% (1.5–1.62 GHz), corresponding to 1.575 GHz. The measured -10-dB impedance bandwidth of port 2 is 18.1% (1.445–1.73 GHz). Thus, the overlapping -10-dB impedance bandwidth for both ports is 7.6% and is limited by port 1. The measured mutual coupling between ports 1 and 2 is lower than -26 dB in the overlapping bandwidth.

Fig. 8 shows the simulated and measured ARs of ports 1 and 2. The AR values for the curves of port 1 (omnidirectional pattern) are the average values of ARs at $\theta = 90°$ plane. It can be observed that the measured AR of port 1 is less than 3 dB in the whole -10-dB impedance bandwidth of port 1. The measured 3-dB AR bandwidth of port 2 (broadside pattern) is 10.2% (1.515–1.675 GHz), which is also within the -10-dB impedance bandwidth of port 2. Based on an overall consideration of the results in Fig. 7 and Fig. 8, the measured
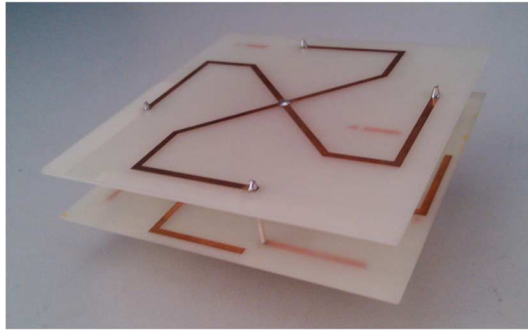
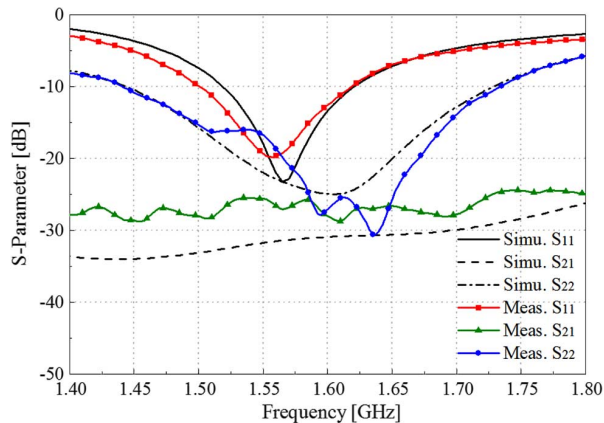Fig. 6.   Photograph of the fabricated pattern diversity antenna.

Fig. 7.   Simulated and measured S-parameters of the CP pattern antenna.
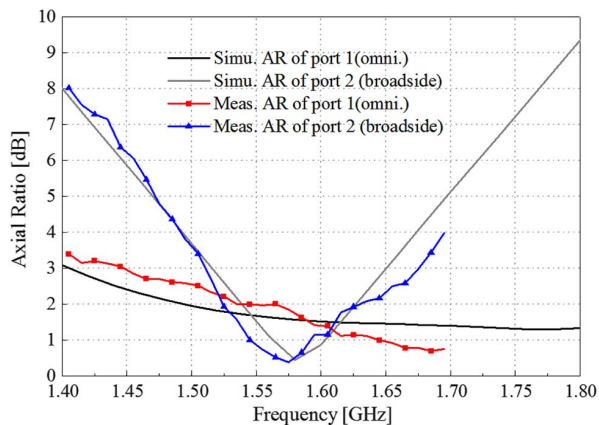

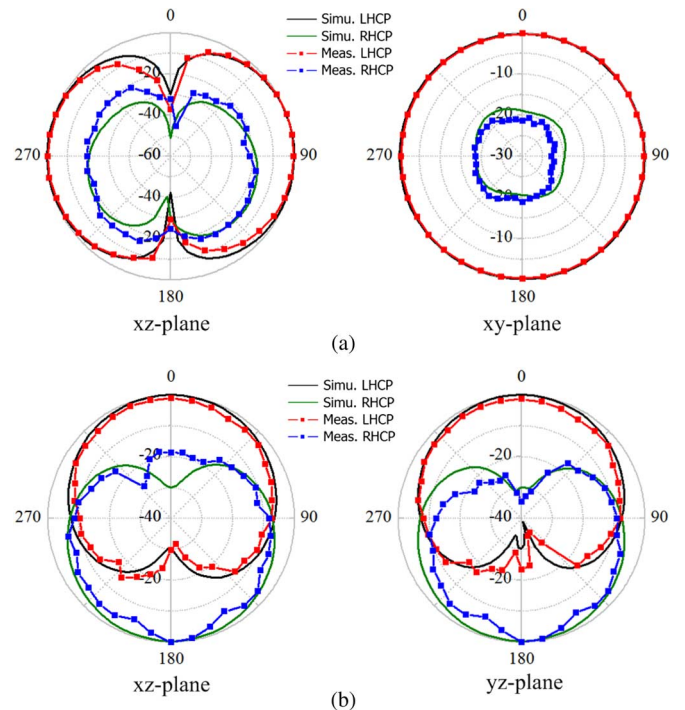Fig. 8.   Simulated and measured ARs of the CP pattern antenna.

Fig. 9.   Simulated and measured normalized radiation patterns at 1.575 GHz. (a) Omnidirectional pattern; (b) broadside pattern.
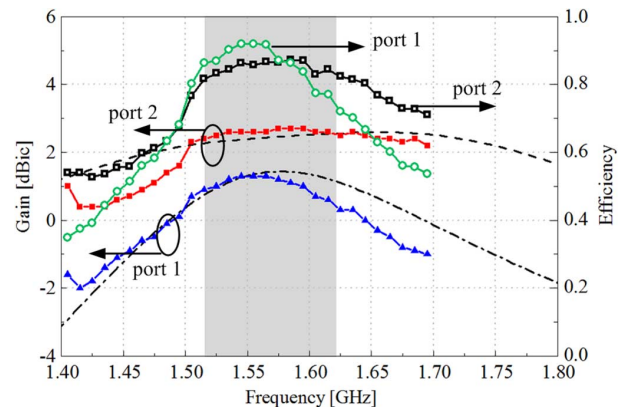

Fig. 10.   Measured realized gains and efficiencies.

region below the lower layer to reduce back lobe in practical applications. The measured gains and efficiencies of both ports are shown in Fig. 10. It is shown that the measured peak gains of port 1 ($\theta = 90^\circ$, $\phi = 0^\circ$) and port 2 ($\theta = 0^\circ$) are about 1.3 dBic and 2.7 dBic, respectively. The efficiencies of ports 1 and 2 are higher than 77% across the usable band.

Fig. 11 shows the measured AR distributions of broadside and omni-directional patterns for upper hemisphere at 1.575 GHz. The measurement method of AR is based on [19], which only needs three components. That is, the maximum magnitudes of the x and y components and phase difference between the two electric components. This method will lead AR variation at $\theta = 0^\circ$. However, this error is acceptable. If the criterion of switching between the two patterns is defined as $\theta = 40^\circ$, 3-dB AR coverage is fully satisfied in $\theta = 40^\circ \sim 90^\circ$ for omnidirectional mode and mainly satisfied in $\theta = 0^\circ \sim 40^\circ$ for broadside mode. Fig. 12 shows the measured LHCP gain distribution. Based on the criterion of $\theta = 40^\circ$, LHCP gain varies from -1 dBic to

overlapping bandwidth for both ports with a criterion of reflection co-efficient < -10 dB and AR < 3 dB is 6.7% (1.515–1.62 GHz), which covers the L1 frequency band of GPS, GLONASS and GALILEO.

The simulated and measured normalized radiation patterns of both modes at 1.575 GHz are shown in Fig. 9, and good agreements between them are observed. Fig. 9(a) shows that the radiation pattern of port 1 is omnidirectional, which has a '∞' shaped in the xz-plane and uniform gain distribution in the xy-plane. The measured LHCP (co-polariza-tion) gain at $\theta = 90^\circ$ plane is 17 dB higher than the RHCP (cross-po-larization) gain. Fig. 9(b) shows that the radiation pattern of port 2 is broadside. It is preferable to introduce lossy absorber material in the
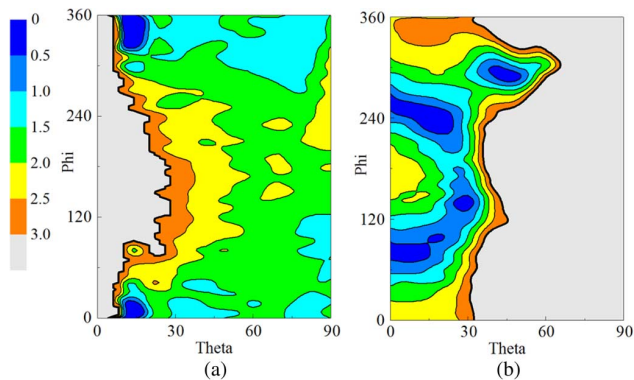
Fig. 11.   Measured AR distribution at 1.575 GHz. (a) Omnidirectional pattern; (b) broadside pattern.
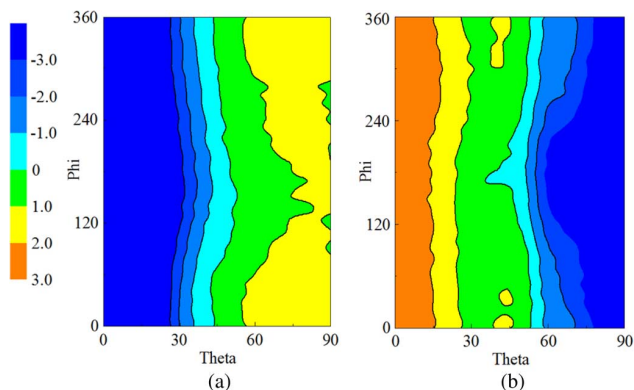

Fig. 12.   Measured LHCP gain distribution at 1.575 GHz. (a) Omnidirectional pattern; (b) broadside pattern.

2 dBic for omnidirectional mode and varies from 0 dBic to 3 dBic for broadside mode.

IV. CONCLUSION

A compact CP pattern diversity antenna is presented in this communication for upper hemispherical coverage. Two collocated antenna elements, one radiating a CP omnidirectional pattern and the other radiating a CP broadside pattern, are integrated in a small volume of $0.38\lambda \times 0.38\lambda \times 0.071\lambda$. Hemispherical coverage is achieved by switching between the two patterns. Acceptable AR (less than 3 dB) and LHCP gain (higher than -1 dBic) are achieved over the entire upper hemisphere. The measured overlapping frequency range of -10-dB impedance bandwidth and 3-dB AR bandwidth for both modes is from 1.515 to 1.62 GHz (6.7%) also with high isolation. Therefore, the proposed diversity antenna present a wideband and low profile alternative of QHA.

REFERENCES

[1] D. Biswas, S. K. N. Patel, and V. Ramachandra, "An airborne antenna system for broadside coverage with varying roll and pitch angles," in *Proc. Applied Electromagnetics Conf.*, 2007, pp. 1–4.

[2] Y. Li, Z. Zhang, and Z. Feng, "A sequential-phase feed using a circularly polarized shorted loop structure," *IEEE Trans. Antennas Propag.*, vol. 61, no. 3, pp. 1443–1447, March 2013.

[3] J. M. Tranquilla and S. R. Best, "A study of the quadrifilar helix antenna for global positioning system (GPS) applications," *IEEE Trans. Antennas Propag.*, vol. 38, no. 10, pp. 1545–1550, 1990.

[4] J. C. Louvigne and A. Sharaiha, "Broadband tapered printed quadrifilar helical antenna," *Electron. Lett.*, vol. 37, pp. 932–933, 2001.

[5] Y. Wang, Y. Sun, and H. Yang, "Analysis and design of a satellite-borne wide-beam conical quadrifilar helical antenna," *Signals Syst. Electron. (ISSSE)*, pp. 1–3, 2010.

[6] M. Caillet, M. Clenet, A. Sharaiha, and Y. M. M. Antar, "A broadband folded printed quadrifilar helical antenna employing a novel compact planar feeding circuit," *IEEE Trans. Antennas Propag.*, vol. 58, no. 7, pp. 2203–2209, 2010.

[7] S. Hebib, N. J. G. Fonseca, P. A. Faye, and H. Aubert, "Compact printed quadrifilar helical antenna with shaped pattern and high cross polarization discrimination," *IEEE Antennas Wireless Propag. Lett.*, vol. 10, pp. 635–638, 2011.

[8] S. L. S. Yang and K. M. Luk, "Design a wide-band L-probe patch antenna for pattern reconfigurable or diversity applications," *IEEE Trans. Antennas Propag.*, vol. 54, no. 2, pp. 433–438, Feb. 2006.

[9] S. L. S. Yang, K.-M. Luk, H.-W. Lai, A. A. Kishk, and K. F. Lee, "A dual-polarized antenna with pattern diversity," *IEEE Antennas Propag. Mag.*, vol. 50, no. 6, pp. 71–79, Dec. 2008.

[10] W. K. Toh, Z. N. Chen, X. Qing, and T. See, "A planar UWB diversity antenna," *IEEE Trans. Antennas Propag.*, vol. 57, no. 11, pp. 3467–3473, Nov. 2009.

[11] K. Wei, Z. Zhang, W. Chen, and Z. Feng, "A novel hybrid-fed patch antenna with pattern diversity," *IEEE Antennas Wireless Propag. Lett.*, vol. 9, pp. 562–565, 2010.

[12] W. L. Liu, T. R. Chen, S. H. Chen, and J. S. Row, "Reconfigurable microstrip antenna with pattern and polarisation diversities," *Electron. Lett.*, vol. 43, no. 2, pp. 77–78, Jan. 18, 2007.

[13] F. Thudor and A. Louzir, "An extremely compact pattern diversity antenna for WLAN," in *Proc. IEEE AP-S Int. Symp.*, Jun. 2002, vol. 4, pp. 60–63.

[14] W. W. Li and K. W. Leung, "Omnidirectional circularly polarized dielectric resonator antenna with top-loaded Alford loop for pattern diversity design," *IEEE Trans. Antennas Propag.*, vol. 61, no. 8, pp. 4246–4256, 2013.

[15] S. Lin and Y. Lin, "A compact sequential-phase feed using uniform transmission lines for circularly polarized sequential-rotation arrays," *IEEE Trans. Antennas Propag*, vol. 59, no. 7, pp. 2721–2724, 2011.

[16] G. H. Brown and O. M. Woodward, "Circularly-polarized omnidirectional antenna," *RCA Rev.*, vol. 8, pp. 259–269, 1947.

[17] Y. M. Pan and K. W. Leung, "Wideband omnidirectional circularly polarized dielectric resonator antenna with parasitic strips," *IEEE Trans. Antennas Propag.*, vol. 60, no. 6, pp. 2992–2997, Jun. 2012.

[18] C. Deng, Y. Li, Z. Zhang, and Z. Feng, "A wideband isotropic radiated planar antenna using sequential rotated L-shaped monopoles," *IEEE Trans. Antennas Propag.*, vol. 62, no. 3, pp. 1461–1464, Mar. 2014.

[19] A. B. Constantine, *Antenna Theory: Analysis and Design*.   New York, NY, USA: Wiley-Interscience, 2005, pp. 73–74.